# Thermodynamics of the Atomic Distribution in $Pt_3Pd_2$, $Pt_2Pd_3$ and their Corresponding (111) Surfaces

**Kyle Meerholz[a] §, David Santos-Carballal[b,c,d], Umberto Terranova[b,e], Anzel Falch[f], Cornelia G.C.E. van Sittert[a,*] and Nora H. de Leeuw[b,d,g,*]**

[a]*Laboratory for Applied Molecular Modelling, Research Focus Area: Chemical Resource Beneficiation (CRB), North-West University, Private Bag X6001, Potchefstroom 2520, South Africa.*

[b]*School of Chemistry, Cardiff University, Main Building, Park Place, Cardiff CF10 3AT, United Kingdom.*

[c]*Materials Modelling Centre, School of Physical and Mineral Sciences, University of Limpopo, Private Bag X1106, Sovenga 0727, South Africa.*

[d]*School of Chemistry, University of Leeds, Leeds LS2 9JT, United Kingdom.*

[e]*School of Postgraduate Medicine and Allied Health, University Buckingham, Crewe Campus, CW1 5DU, United Kingdom.*

[f]*Electrochemistry for Energy & Environment Group, Research Focus Area: Chemical Resource Beneficiation (CRB), North-West University, Private Bag X6001, Potchefstroom 2520, South Africa.*

[g]*Department of Earth Sciences, Utrecht University, Princetonplein 8A, 3584 CB Utrecht, Netherlands.*

Received 9 March 2020, revised 9 September 2020, accepted 23 September 2020.

**ABSTRACT**

**In this study, we have developed solid-state models of platinum and palladium bimetallic catalysts, $Pt_3Pd_2$ and $Pt_2Pd_3$, which are rapidly thermally annealed at 800 °C. These models were constructed by determining all the unique atomic configurations in a 2 × 2 × 1 supercell, using the program Site-Occupation Disorder (SOD), and optimized with the General Utility Lattice Program (GULP) using Sutton-Chen interatomic potentials. Each catalyst had 101 unique bulk models that were developed into surface models, which were constructed using the two-region surface technique before the surface energies were determined. The planes and compositions with lowest surface energies were chosen as the representative models for the surface structure of the bimetallic catalysts. These representative models will now be used in a computational study of the HyS process for the production of hydrogen.**

**KEYWORDS**

**HyS process, platinum, palladium, solid-state, catalyst, Site-Occupation Disorder.**

## 1. Introduction

As research into alternative energy becomes increasingly important, hydrogen has been proposed as a potential replacement for hydrocarbon fuels.[1] Hydrogen has the advantages of being environmentally friendly, readily available and possessing a high energy density.[2] However, hydrogen as replacement fuel is held back by many challenges, including storage and production technology shortfalls. A current industrial-scale hydrogen production method is electrolysis, where water is split into hydrogen and oxygen. Unfortunately, water splitting using electrolysis is an energy-intensive process, and the goal is therefore to create more efficient and environmentally sound routes to produce hydrogen. One such route could be the hybrid sulphur (HyS) process, which was first proposed by the Westinghouse Corporation.[3] The HyS process produces hydrogen *via* the electro-oxidation of aqueous $SO_2$ at the anode of an $SO_2$ depolarized electrolyzer (SDE).[4] Various metal catalysts (platinum, palladium and gold), serving as the anode in the SDE, have been reviewed by Díaz-Abad *et al.*[5] Platinum was shown to be the most effective catalyst, with a high catalyst activity and high resistance to corrosion in the acidic environment present at the anode. However, scarcity and cost are major fundamental limitations associated with Pt, and research into lowering the amount of platinum used in catalysts is therefore vital if hydrogen is to become a viable replacement energy source.

One study into alternative platinum-based catalysts was carried out by Falch *et al.*[6] who found potential replacement catalysts by depositing multi-metal thin films through physical vapour deposition onto glassy carbon electrodes as the substrate. The study showed that thin-film combinations of $Pt_3Pd_2$ and $Pt_2Pd_3$ were two of the best performing catalyst as anode materials for $SO_2$ oxidation, achieving onset potentials of 0.587 V and 0.590 V, respectively.[6] The onset potentials of these catalysts compare well with the value reported for standard platinum as the catalyst (0.598 V),[7] whilst using less expensive alloys. However, one problem related to these catalysts is the tendency of the thin metal films to delaminate, to certain degrees, from the glassy carbon surface during testing. This problem was addressed by rapid thermal annealing at 800 °C, which reduced the delamination phenomenon and increased stability.[4,8] It was shown that the annealing drastically changes the surface structure of the catalysts, which results in the improved durability of the catalyst. The XRD analysis of the catalysts indicates that the (111) Miller plane peak increases with annealing temperature, while the (200) and (311) planes, as identified by Mahapatra and Datta,[9] remain mostly unchanged. The (111) peak also correlates well with the catalyst activity,[10] indicating that this (111) surface enables active site formation. These potential replacement catalysts perform to a similar degree as the standard platinum catalysts in terms of activity, but they have a longer life-time compared to the standard platinum catalysts.[8a]

Given the promise of Pd/Pt alloys as catalysts in the HyS

* To whom correspondence should be addressed.
E-mail: C.G.C.E.v.S., cornie.vansittert@nwu.ac.za / N.H.d.L., n.h.deleeuw@leeds.ac.uk

ISSN 0379-4350 Online / ©2021 South African Chemical Institute / http://saci.co.za/journal
DOI: https://doi.org/10.17159/0379-4350/2021/v74a7

process, this study aims to develop solid-state models of platinum and palladium bimetallic catalysts, $Pt_3Pd_2$ and $Pt_2Pd_3$, annealed at 800 °C to be used in the modelling of the HyS process for the production of hydrogen. To this end, we will identify and construct the most stable $Pt_3Pd_2$ and $Pt_2Pd_3$ bi-metallic bulk material, followed by the creation of (111) surface models.

## 2. Computational Methods

Various bulk configurations, at the desired ratios of $Pt_3Pd_2$ and $Pt_2Pd_3$, were constructed by substitution of Pd into all available sites of the pure Pt bulk and *vice versa*, using the program Site-Occupation Disorder (SOD)[11] in a similar manner to the recent study conducted by Botha *et al*.[12] The unit cells of Pt and Pd were constructed with F-type lattice, in a face-centred cubic (*fcc*) cell with space group Fm-3m (number 225) by entering the crystallographic properties into SOD. The cell size was limited to a 2 × 2 × 1 supercell as larger supercells were unfeasible due to the large numbers of configurations generated for the different alloy compositions that would need to be considered, which would be beyond the computational capabilities of the SOD program. In this instance, SOD can treat a 2 × 2 × 1 cell with 16 atoms within a reasonable timeframe. However, a 2 × 2 × 2 cell with 32 atoms leads to so many different configurations, that its computation cannot be completed within a sensible timeframe.[13] The unit cell of Pt was expanded into a 2 × 2 × 1 rectangular cell with *a* and *b* lengths of 7.847 Å and *c* of 3.924 Å, and cell angles of 90.0 °, based on the lattice constant at 25 °C obtained from Arblaster.[14] The Pd cell had lengths *a*, *b* of 7.780 Å and *c* with a length of 3.890 Å, and cell angles of 90.0 °, again based on lattice constants at 25 °C obtained from Arblaster.[15] In addition to generating all inequivalent distribution configurations for each alloy composition, SOD also provided various properties and energies of each bulk configuration, i.e. Boltzmann probability distributions, bulk energies and thermodynamic energies at different temperatures. The temperatures used were in the range of –272 °C to 900 °C, as 900 °C was the highest temperature used in the annealing of the catalysts as reported by Falch *et al*.[8a] The optimized structures were analyzed, and the most probable bulk configurations determined using the Boltzmann probabilities. The list of configurations obtained from SOD was geometry optimized using the molecular mechanics based General Utility Lattice Program (GULP),[16] with the interatomic potentials from the Sutton-Chen library of potentials.[17] The geometry optimization was carried out under constant pressure, until the equilibrium volume was reached.

The surface energies for Pt, Pd and all 101 inequivalent configurations for both $Pt_3Pd_2$ and $Pt_2Pd_3$ catalysts were calculated. However, before the surface energies could be calculated the cubic symmetry of the bulk was re-obtained through resizing the bulk to a 2 × 2 × 2 cell by doubling in the z-direction, thereby increasing the simulation cells to 32 atoms. The $Pt_3Pd_2$ bulk materials now contained 12 Pd and 20 Pt atoms, with cell dimensions of 7.8472 Å and cell angles of 90.0 °. The $Pt_2Pd_3$ bulks now contained 12 Pt and 20 Pd atoms, with cell dimensions of 7.7804 Å and cell angles of 90.0 °. Slab structures without dipole were created using the program METADISE[18] (minimum energy techniques applied to dislocation interface and surface energies), to cut geometrically optimized bulk structures along the (111) Miller plane. Additionally, METADISE was used to determine the symmetrical terminations of each configuration, which is required for the determination of the surface energies.[19] The surface energy was determined by employing a two-region method[18], as shown in Fig. 1. Region 1 represents the atoms near the surface which are all allowed to relax fully, while Region 2

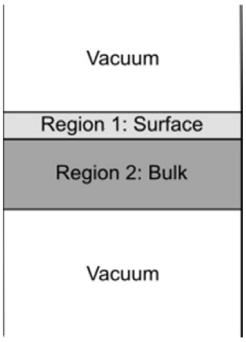


**Figure 1** A visualization of the two-region method, illustrating the surface model with surface layer (Region 1) and bulk layer (Region 2) and the vacuum layers surrounding them.

represents the rest of the bulk material where the atoms are kept fixed in their bulk-optimized positions.[13,20] The addition of Region 2 is necessary to ensure that the potentials acting on the atoms in Region 1 at the interface with Region 2 and close to the surface are modelled correctly. The surface thickness (Region 1) and the bulk thickness (Region 2) must be optimized to model a sufficiently large system to achieve convergence and increase accuracy, whilst keeping the system small enough to minimize computing time. This optimization was done for one of the configuration structures and assumed to be the same for the remainder of the compositional configurations.

The total energy of a surface ($U_{Total}$), consisting of the two regions, is calculated using Equation (1), where the subscript denotes the interactions between the regions. However, the energy of Region 2 ($U_{22}$) is not required as it is cancelled out in the surface energy calculations, as it describes the energy of an infinitely large bulk below the surface, but it is required to obtain convergence of the calculations. To calculate the energy of the relaxed surface ($U_{Surface}$), the energy of Region 1 ($U_{11}$) and half the energy interaction between Region 1 and Region 2 ($U_{12}$) is required, as shown in Equation (2). The surface energy ($\Delta U_{SE}$), written in terms of Equation (3), can now be calculated by subtraction of the bulk energy ($U_{Bulk}$) from the energy of the $U_{Surface}$ per unit surface area (A). $U_{Bulk}$ is obtained by multiplying the energy value of the original 16-atom cell by the number of times this cell is occurs in Region 1 and Region 2. A lower positive value for the surface energy ($\Delta U_{SE}$) of a solid indicates a more thermodynamically stable surface.[13]

$$U_{Total} = U_{11} + U_{12} + U_{22} \quad (1)$$

$$U_{surface} = U_{11} + \left(\frac{U_{12}}{2}\right) \quad (2)$$

$$\Delta U_{SE} = \left(\frac{U_{surface} - U_{bulk}}{A}\right) \quad (3)$$

To validate the surface energy calculations, surface energies of the pure Pt and Pd metals were calculated and compared to values reported in the literature. The Pt and Pd bulk metals were constructed using the same process that was used to create the bulk of the $Pt_3Pd_2$ and $Pt_2Pd_3$. Both Pt and Pd bulks were optimized and cut along the (111) Miller plane and constructed into surface models with the same Region 1 and 2 thicknesses as stated earlier. Surface energies of Pt (0.90 J m$^{-2}$) and Pd (0.99 J m$^{-2}$), as reported by Todd and Lynden-Bell[21] were obtained using a similar method and also employing the Sutton-Chen interatomic potentials. Similarly, Kimura *et al*.[22] reported surface energies, using Sutton-Chen potentials, for Pt and Pd at 0.913 J m$^{-2}$ and 1.003 J m$^{-2}$.

## 3. Results

In the model of the $Pt_3Pd_2$ catalyst with the desired concentration of Pt 60.0 % Pd 40.0 %, a total of 6 out of the 16 Pt atoms in the bulk were substituted by Pd using the SOD program, which led to a Pt concentration of 62.5 % and Pd of 37.5 %. Similarly, the $Pt_2Pd_3$ model was constructed by replacing 6 Pd atoms with Pt in the Pd bulk giving concentrations of Pd at 62.5 % and Pt 37.5 %. These model concentrations are similar to the composition of the experimental results, as reported by Falch *et al*.[6] For both models, SOD generated 8008 possible configurations, but of those only 101 were unique. SOD uses Boltzmann probabilities to predict which configurations are likely to occur at specific temperatures and these probability predictions were used to further reduce the number of required bulk calculations by focussing only on the configurations which are likely to occur at the desired temperature; in this study, a probability threshold of 1 % was used. Figure 2 indicates the number of bulk configurations that are probable at temperatures ranging from –272 °C to 900 °C for both $Pt_3Pd_2$ and $Pt_2Pd_3$ systems.

At –272 °C, only one configuration is probable in each catalyst, which correlates to the lowest-energy configuration. However, as the temperature increases, the number of configurations increases slowly to 12 and 6 configurations at –72 °C for $Pt_3Pd_2$ and $Pt_2Pd_3$, respectively. $Pt_3Pd_2$ shows an exponential increase in the number of configurations between 0 °C and 400 °C from 28 to 94 configurations, until the maximum number of configurations, namely 101 configurations, is reached at 800 °C. In terms of $Pt_2Pd_3$, the rate at which the number of configurations grows is much slower, only reaching 95 at 900 °C. This difference in the number of configurations between the two compositions would suggest that the $Pt_2Pd_3$ catalyst requires higher annealing temperatures to achieve more random configurations. However, in experimental work[6] these catalysts are rapidly thermally annealed at 800 °C, and, as illustrated, all 101 inequivalent bulk configurations of $Pt_3Pd_2$ and 94 of $Pt_2Pd_3$ are probable at this temperature. For the sake of completeness and comparison, it was decided to investigate all 101 configurations for both systems.

Table S1 and Table S2 found in the supplementary information, list the ten most likely configurations at different temperatures of the $Pt_3Pd_2$ and $Pt_2Pd_3$ systems, respectively. Included in the tables are relative bulk energies and Boltzmann probabilities. These tables indicate how the distribution of the configurations is spread more evenly as the temperature increases, highlighting the necessity to take into account not only lowest-energy configurations but also higher energy configurations which become probable at the annealing temperatures. For example, at 25 °C configuration 94 of the $Pt_3Pd_2$ catalyst has a probability of 25.36 % (highest probability configuration), but at 800 °C, it has fallen to sixth position with a probability of only 3.55 %, even though it is the bulk configuration with the lowest energy. This behaviour can be explained by the level of the degeneracy of the different configurations; a higher degeneracy will allow a configuration to become more probable at higher temperatures. In the case of the $Pt_2Pd_3$ catalyst, the lowest-energy configuration, namely 94, remains the most probable configuration as predicted by the Boltzmann probabilities. This suggests that the other configurations do not have a high enough degeneracy, or their relative energies are too high to compete effectively with configuration 94 to become the most likely configuration in the distribution. However, we note that the differences between the relative bulk energies, of the configurations, are less than 0.1 kJ, supporting the conclusion that at higher temperatures a larger number of configurations becomes accessible. However, the Boltzmann probability of the bulk configurations is complemented by a description of the surface energies to identify the ground state configuration.

First, surface energy calculations were carried out on different sizes of Regions 1 and 2. Figure 3 shows the results of varying the sizes of Region 1 and Region 2, using the bulk of $Pt_3Pd_2$ configuration 1 as a representative example. For Region 1 the surface energy is stable at 3 –4 layers, however, it was decided to double the thickness to seven layers for all proceeding surface energy calculations to ensure convergence for the remainder of configurations. Region 2 shows stability at five layers and again it was doubled in thickness to 10 layers for all surface energy calculations, to ensure that the system converges with the remainder of configurations.

Hence all subsequent surfaces were constructed with a Region 1 with 7 layers and Region 2 with 10 layers. The surface energies of the pure Pt and Pd metals were calculated first, with Pt giving a surface energy of 0.925 J $m^{-2}$ and Pd one of 1.039 J $m^{-2}$. These results compare well to the reported values from Todd and Lynden-Bell[21] of Pt 0.90 J $m^{-2}$ and Pd 0.99 J $m^{-2}$. Additionally they

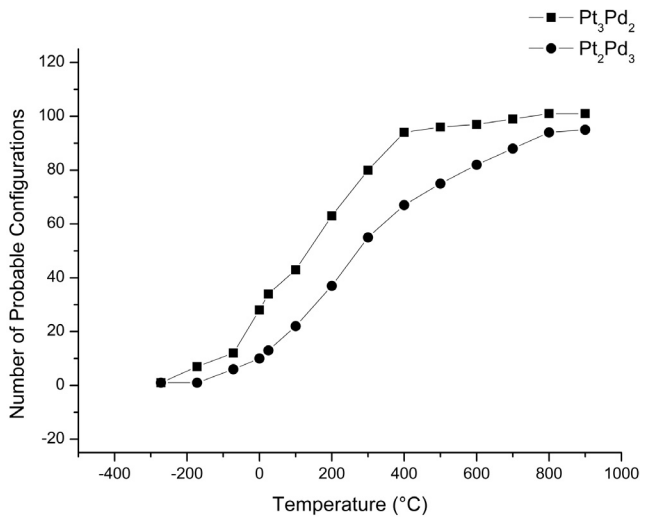


**Figure 2** The number of bulk configurations probable in relation to temperature, of $Pt_3Pd_2$ and $Pt_2Pd_3$ in a 2 × 2 × 1 cell as predicted by SOD.

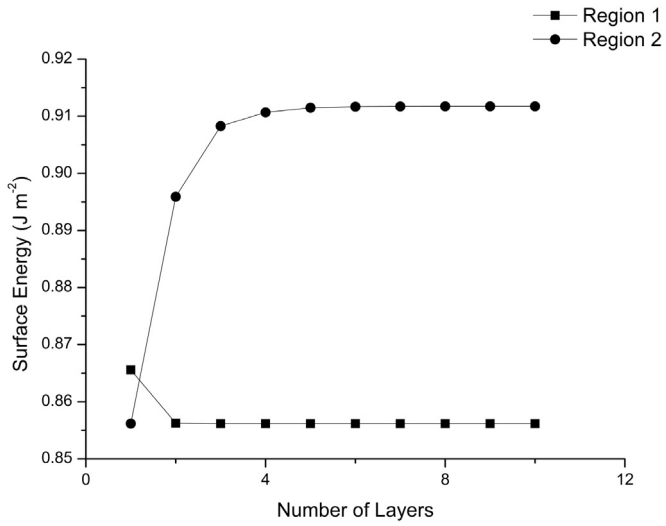


**Figure 3** Surface energy optimization of $Pt_3Pd_2$ by varying the Region thickness of configuration 1 at 800 °C. Initially, Region 2 was held constant at 10 layers while testing Region 1, after which Region 1 was held constant at sevenlayers and Region 2 was varied.

correspond to the values reported by Kimura *et al.*,[22] at Pt 0.913 J m$^{-2}$ and Pd 1.003 J m$^{-2}$, indicating the validity of the method and accuracy of the calculated surface energies.

The calculated surface energies of the two catalyst systems are displayed in Fig. 4 and Fig. 5. The surface energies for $Pt_3Pd_2$ vary from 0.817 J m$^{-2}$ to 1.007 J m$^{-2}$, with configuration 3 considerably more stable (lower surface energy) than the rest of the configurations, which will, therefore, be the most likely representative surface configuration of the $Pt_3Pd_2$ surface. The surface energy results for the $Pt_2Pd_3$ vary less between the minimum and maximum values with an energy range of 0.887 J m$^{-2}$ to 1.007 J m$^{-2}$. There is a group of three configurations that are notably more stable than the rest of the 101 configurations, i.e. configurations 17, 81 and 8 with energies calculated at 0.887 J m$^{-2}$, 0.888 J m$^{-2}$ and 0.889 J m$^{-2}$, respectively. These configurations will, therefore, most likely occur in the surface structure of the $Pt_2Pd_3$ model.

described in the following in notation, in which the square brackets denote the beginning and end of a sequence and the round brackets denote the individual rows, as seen from left to right. Figure 6a shows $Pt_3Pd_2$ configuration 3, the surface structure consists of a row with the following sequence [(Pt), (Pd-Pd-Pd-Pt)]. Figure 6b shows $Pt_2Pd_3$ configuration 17, the surface structure contains the following sequence [(Pt-Pt-Pd-Pd), (Pd-Pd-Pd-Pt), (Pd-Pt), (Pd-Pd-Pd-Pt)]. Figure 6c shows $Pt_2Pd_3$ configuration 81, with the following surface structure [(Pt-Pd-Pd-Pd), (Pt-Pd)]. Figure 6d shows $Pt_2Pd_3$ configuration 8 with the surface structure with the following sequence [(Pt-Pd), (Pd), (Pt), (Pd)]. The top layer arrangement was highlighted to see if any correlation between configurations, which would explain the reason for the lower surface energies. However, as can be seen, the configurations show no correlation to one another, and there are no obvious similarities between them.

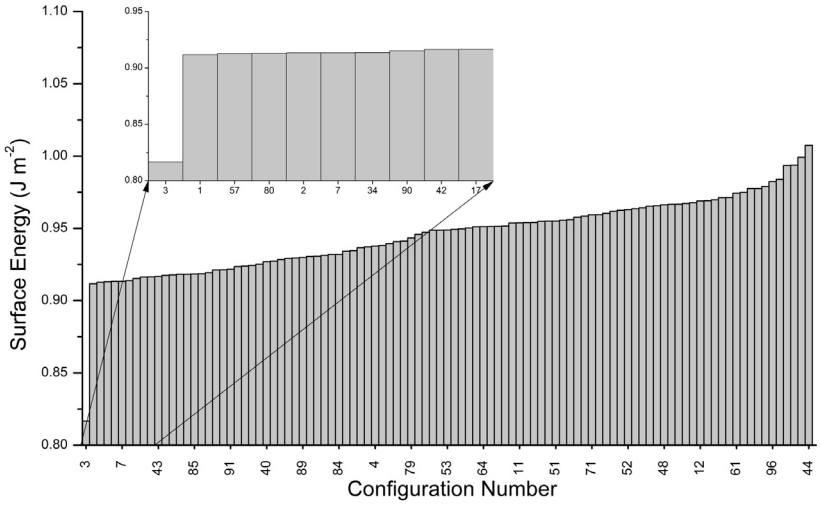


**Figure 4** Surface energies for the 101 configurations of the $Pt_3Pd_2$ catalyst arranged in ascending order, the first 10 configurations are show in more detail in the expanded section.

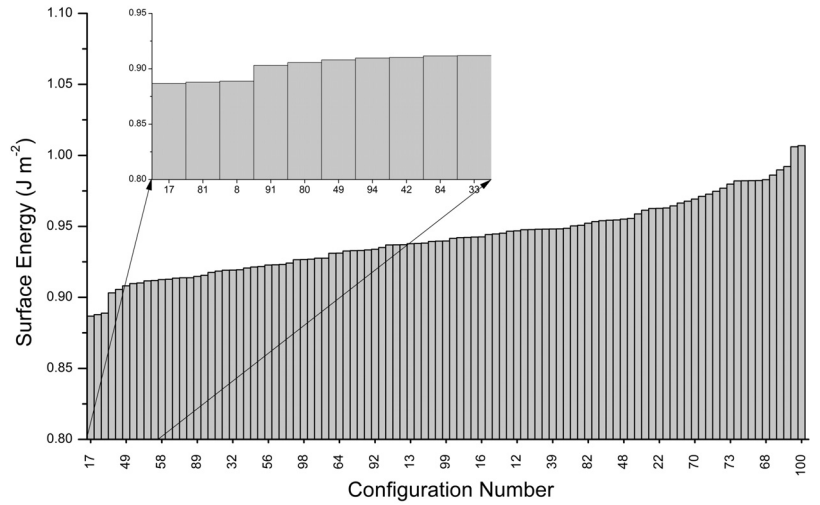


**Figure 5** Surface energies for the 101 configurations of the $Pt_2Pd_3$ catalyst arranged in ascending order, the first 10 configurations are show in more detail in the expanded section.

The four best performing surface configurations, as listed above, visualizations of the top layer of the surfaces are shown in Fig. 6. The surface area of each configuration has been quadrupled in size, by doubling the lengths of *a* and *b*, of the periodic cell. This was done to easily identify the arrangement of Pt and Pd, and determine the atomic sequences. The sequences are

## 4. Conclusions

This study aimed to construct solid-state models of two bi-metallic catalysts, namely $Pt_3Pd_2$ and $Pt_2Pd_3$, which could then be used in the modelling of the HyS process for the production of hydrogen. The bulk materials for both catalyst compositions were constructed by using the program SOD to create

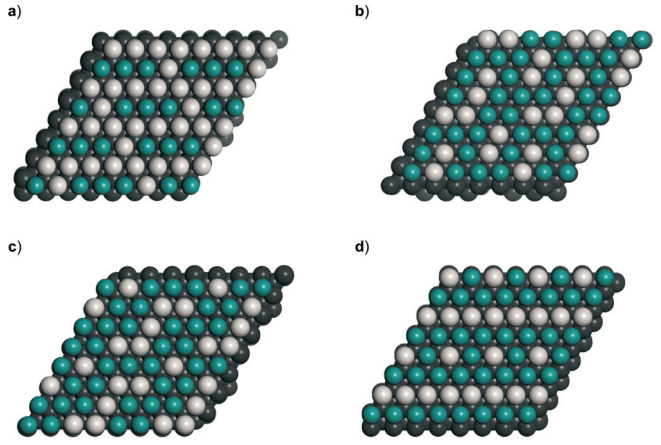


**Figure 6** A selection of visualizations of the lowest surface energies of $Pt_3Pd_2$ and $Pt_2Pd_3$ catalysts. (**a**) Visualization of $Pt_3Pd_2$ configuration 3; (**b**) visualization of $Pt_2Pd_3$ configuration 17; (**c**) visualization of $Pt_2Pd_3$ configuration 81; (**d**) visualization of $Pt_2Pd_3$ configuration 8.

unique bulk configurations by replacing single atoms from the pure metal by the alloying metal. The unit cell of the two compositions produced a total of 8008 configurations with 101 unique configurations for both $Pt_3Pd_2$ and $Pt_2Pd_3$ systems. The results obtained from the bulk calculations indicated that all 101 configurations had to be considered, as the high-temperature annealing process of the catalysts would allow most of the configurations to occur. Hence, another method of choosing a representative surface model was needed.

Thus, we created surface models from the different bulk configurations, which were used to calculate the surface energies of each of the catalyst systems, with the configurations with the lowest surface energies selected as being representative of the catalyst surface. These surfaces were not constructed from the bulk configuration with the lowest energy, justifying our decision to select the representative surface configurations based on their surface energies. This method of calculating surface energies using Sutton-Chen interatomic potentials, was validated by comparing the surface energies of the pure metal systems against those reported in the literature, with good agreement between our results and the literature values. The calculated surface energies of the $Pt_3Pd_2$ catalyst indicate that one configuration had notably lower surface energy and is hence a significantly more stable surface than the rest, with a surface energy of 0.817 J $m^{-2}$; visualizations and Cartesian coordinates can be found in Fig. S1 in the supplementary information. The $Pt_2Pd_3$ system had three configurations with comparable low energies, calculated at 0.887 J $m^{-2}$, 0.888 J $m^{-2}$ and 0.889 J $m^{-2}$, respectively, and shown in Figs. S2–S4 in the supplementary information.

The stacking sequences of the four lowest energy surfaces show no evident correlation or similarities, which indicates that the minor differences in surface energy that occur are caused by nearest-neighbour interactions. As the compositions of each of the surfaces remain the same, only these configurational differences can be the reason for the variations in surface energies. However, due to the classical nature of interatomic potential-based simulations, electronic properties of the surfaces cannot be obtained. Future work should therefore include investigations of these surface models using quantum mechanical techniques, such as calculations based on the Density Functional Theory.

## Acknowledgements

We thank the UK Economic and Social Research Council (ESRC Grant ES/N013867/1) and the National Research Foundation of South Africa for a UK/SA PhD exchange grant under the Newton Programme. We further acknowledge the UK Engineering & Physical Sciences Research Council (EPSRC Grants EP/K016288/1 and EP/K009567/2) for funding. This work was performed using the computational facilities of the Advanced Research Computing @ Cardiff (ARCCA) Division, Cardiff University, and the Supercomputing Facilities at Cardiff University operated by ARCCA on behalf of the HPC Wales and Supercomputing Wales (SCW) projects. We acknowledge the support of SCW, which is part-funded by the European Regional Development Fund (ERDF) *via* the Welsh Government. The authors also acknowledge the use of the resources of the Centre for High-Performance Computing (CHPC) of South Africa in the completion of this work. D.S.-C. is grateful to the Department of Science and Technology (DST) and the National Research Foundation (NRF) of South Africa for the provision of a Postdoctoral Fellowship for Early Career Researchers from the United Kingdom. All data created during this research are openly available from the Cardiff University's Research Portal http://doi.org/10.17035/d.2020.0102731858

## Supplementary material

A supplementary document is available with this article that has additional information of the results obtained from the SOD program. Additionally, the supplementary document gives the Cartesian coordinates and visualizations of the four lowest surface energy configurations, namely $Pt_3Pd_2$ configuration 3 and $Pt_2Pd_3$ configurations 8, 17 and 81 and including the across and onto views of these surfaces.

**[§]ORCID iDs**
K. Meerholz: orcid.org/0000-0002-5873-4563
D. Santos-Carballal: orcid.org/0000-0002-3199-9588
A. Falch: orcid.org/0000-0002-9771-5699
C.G.C.E. van Sittert orcid.org/0000-0001-5786-5409
N.H. de Leeuw: orcid.org/0000-0002-8271-0545

## References

1 a) T.N. Veziroglu and F. Barbir, Hydrogen: the wonder fuel, *Int. J. Hydrogen Energy*, 1992, **17**, 391–404; b) D. Mori and K. Hirose, Recent challenges of hydrogen storage technologies for fuel cell vehicles, *Int. J. Hydrogen Energy*, 2009, **34**, 4569–4574; c) M. Momirlan and T.N. Veziroglu, The properties of hydrogen as fuel tomorrow in sustainable energy system for a cleaner planet, *Int. J. Hydrogen Energy*, 2005, **30**, 795–802.

2 A. Züttel, A. Remhof, A. Borgschulte and O. Friedrichs, Hydrogen: the future energy carrier, *Philos. Trans. Royal Soc. A: Math., Phys. Eng. Sci.*, 2010, **368**, 3329–3342.

3 a) L.E. Brecher, S. Spewock and C.J. Warde, The Westinghouse Sulfur Cycle for the thermochemical decomposition of water, *Int. J. Hydrogen Energy*, 1977, **2**, 7–15; b) W.A. Summers and M.B. Gorensek, *Nuclear Hydrogen Production Based on the Hybrid Sulfur Thermochemical Process*, American Nuclear Society – ANS, United States, 2006; c) C. Sattler, M. Roeb, C. Agrafiotis and D. Thomey, Solar hydrogen production via sulphur based thermochemical water-splitting, *Solar Energy*, 2017, **156**, 30–47.

4 A. Falch, V.A. Badets, C. Labrugère and R.J. Kriek, Co-sputtered $Pt_xPd_yAl_z$ thin film electrocatalysts for the production of hydrogen via $SO_2$(aq) electro-oxidation, *Electrocatalysis*, 2016, **7**, 376–390.

5 S. Díaz-Abad, M. Millán, M.A. Rodrigo and J. Lobato, Review of anodic catalysts for $SO_2$ depolarized electrolysis for "green hydrogen" production, *Catalysts*, 2019, **9**, 63.

6 A. Falch, V. Lates and R.J. Kriek, Combinatorial plasma sputtering of PtxPdy thin film electrocatalysts for aqueous $SO_2$ electro-oxidation, *Electrocatalysis*, 2015, **6**, 322–330.

7 J.A. O'Brien, J.T. Hinkley and S.W. Donne, Electrochemical oxidation of aqueous sulfur dioxide II. Comparative studies on platinum and gold electrodes, *J. Electrochem. Soc.*, 2012, **159**, F585–F593.

8 a) A. Falch, V.A. Lates, H.S. Kotzé and R.J. Kriek, The effect of rapid

thermal annealing on sputtered Pt and $Pt_3Pd_2$ thin film electrocatalysts for aqueous $SO_2$ electro-oxidation, *Electrocatalysis*, 2016, **7**, 33–41; b) A. Falch, *Investigating Sputtered Thin Film Pt-containing Electrocatalysts for $SO_2$ (aq) Electro-oxidation*, PhD thesis, North-West University, Potchefstroom, South Africa, 2016.

9 S.S. Mahapatra and J. Datta, Characterization of Pt-Pd/C electrocatalyst for methanol oxidation in alkaline medium, *Int. J. Electrochem.*, 2011, **2011**, 16.

10 a) I.E.L. Stephens, A.S. Bondarenko, F.J. Perez-Alonso, F. Calle-Vallejo, L. Bech, T.P. Johansson, A.K. Jepsen, R. Frydendal, B.P. Knudsen, J. Rossmeisl and I. Chorkendorff, Tuning the activity of Pt(111) for oxygen electroreduction by subsurface alloying, *J. Am. Chem. Soc.*, 2011, **133**, 5485–5491; b) J. Greeley, J. Rossmeisl, A. Hellmann and J.K. Norskov, Theoretical trends in particle size effects for the oxygen reduction reaction, *Z. Phys. Chem.*, **221**, 2007, 1209; c) S.W. Lee, S. Chen, J. Suntivich, K. Sasaki, R.R. Adzic and Y. Shao-Horn, Role of surface steps of Pt nanoparticles on the electrochemical activity for oxygen reduction, *J. Phys. Chem. Lett.*, 2010, **1**, 1316–1320.

11 R. Grau-Crespo, S. Hamad, C.R.A. Catlow and N.H. de Leeuw, Symmetry-adapted configurational modelling of fractional site occupancy in solids, *J. Physics: Condens. Matter*, 2007, **19**, 256201.

12 L.M. Botha, D. Santos-Carballal, U. Terranova, M.G. Quesne, M.J. Ungerer, C.G.C.E. van Sittert and N.H. de Leeuw, Mixing thermodynamics and electronic structure of the Pt1-xNix ($0 \leq x \leq 1$) bimetallic alloy, *RSC Advances*, 2019, **9**, 16948–16954.

13 G. Watson, E. Toby Kelsey, N. Leeuw, D.J. Harris and S. Parker, Atomistic simulation of dislocations, surfaces and interfaces in MgO, *J. Chem. Soc., Faraday Trans.*, **92**, 1996.

14 J. Arblaster, Crystallographic properties of platinum, *Platinum Met. Rev.*, 1997, **41**, 12–21.

15 J.W. Arblaster, Crystallographic properties of palladium, *Platinum Met. Rev.*, 2012, **56**, 181–189.

16 a) J.D. Gale, GULP: a computer program for the symmetry-adapted simulation of solids, *J. Chem. Soc., Faraday Trans.*, 1997, **93**, 629–637; b) A.L. Rohl, The General Utility Lattice Program (GULP), *Mol. Simulation*, 2003, **29**, 291–341; c) D. Gale Julian, GULP: capabilities and prospects, *Z. Kristallogr. – Crystal. Mater.*, 2005, **220**, 552.

17 J. Chen, Long-range Finnis–Sinclair potentials, *Philos. Mag. Lett.*, 1990, **61**, 139–146.

18 G.W. Watson, E.T. Kelsey, N.H. de Leeuw, D.J. Harris and S.C. Parker, Atomistic simulation of dislocations, surfaces and interfaces in MgO, *J. Chem. Soc., Faraday Trans.*, 1996, **92**, 433–438.

19 P.W. Tasker, The surface energies, surface tensions and surface structure of the alkali halide crystals, *Philos. Mag. A*, 1979, **39**, 119–136.

20 a) D. Santos-Carballal, A. Roldan, R. Grau-Crespo and N.H. de Leeuw, A DFT study of the structures, stabilities and redox behaviour of the major surfaces of magnetite Fe3O4, *Phys. Chem. Chem. Phys.*, 2014, **16**, 21082–21097; b) D. Santos-Carballal, Z. Du, H.E. King and N.H. de Leeuw, A computational study of the interaction of organic surfactants with goethite $\alpha$-FeO(OH) surfaces, *RSC Advances*, 2016, **6**, 91893–91903; c) N.H. de Leeuw, S.C. Parker, H.M. Sithole and P.E. Ngoepe, Modeling the surface structure and reactivity of pyrite: introducing a potential model for $FeS_2$, *J. Phys. Chem. B*, 2000, **104**, 7969–7976.

21 B.D. Todd and R.M. Lynden-Bell, Surface and bulk properties of metals modelled with Sutton-Chen potentials, *Surf. Sci.*, 1993, **281**, 191–206.

22 Y. Kimura, Y. Qi, T. Cagin, W.A. Goddard III, The quantum Sutton-Chen many-body potential for properties of fcc metals, *Caltech ASCI Technical Report 003*, 1998.

## Supplementary material to:

K. Meerholz, D. Santos-Carballal, U. Terranova, A. Falch, C.G.C.E. van Sittert and N.H. de Leeuw,

Thermodynamics of the Atomic Distribution in $Pt_3Pd_2$, $Pt_2Pd_3$ and their Corresponding (111) Surfaces

*S. Afr. J. Chem.,* 2021, **74** (Special Edition), 36–41.

# Supplementary Information, S. Afr. J. Chem.

# Thermodynamics of the Atomic Distribution in $Pt_3Pd_2$, $Pt_2Pd_3$ and their Corresponding (111) Surfaces

Kyle Meerholz,[1] David Santos-Carballal,[2,3,4] Umberto Terranova,[2,5] Anzel Falch,[6] Cornelia G. C. E. van Sittert,[1*] Nora H. de Leeuw[2,4,7*]

[1] Laboratory for Applied Molecular Modelling, Research Focus Area: Chemical Resource Beneficiation (CRB), North-West University, Private Bag X6001, Potchefstroom 2520, South Africa

[2] School of Chemistry, Cardiff University, Main Building, Park Place, Cardiff CF10 3AT, United Kingdom

[3]Materials Modelling Centre, School of Physical and Mineral Sciences, University of Limpopo, Private Bag x1106, Sovenga 0727, South Africa

[4] School of Chemistry, University of Leeds, Leeds LS2 9JT, United Kingdom

[5] School of Postgraduate Medicine and Allied Health, University Buckingham, Crewe Campus, CW1 5DU, United Kingdom

[6] Electrochemistry for Energy & Environment Group, Research Focus Area: Chemical Resource Beneficiation (CRB), North-West University, Private Bag X6001, Potchefstroom 2520, South Africa

[7] Department of Earth Sciences, Utrecht University, Princetonplein 8A, 3584 CB Utrecht, The Netherlands

[*Corresponding Authors E-mails: Cornie.VanSittert@nwu.ac.za; N.H.deLeeuw@Leeds.ac.uk]

Table of Contents

*Table S1: A list of the ten most probable bulk configurations of $Pt_3Pd_2$ predicted by SOD, out of the 101 inequivalent configurations at different temperatures, listing the configuration numbers, relative electronic bulk energies and Boltzmann probabilities*

| Config. No. | 25 °C Relative Energy (kJ) | Probability (%) | Config. No. | 700 °C Relative Energy (kJ) | Probability (%) | Config. No. | 800 °C Relative Energy (kJ) | Probability (%) | Config. No. | 900 °C Relative Energy (kJ) | Probability (%) |
|---|---|---|---|---|---|---|---|---|---|---|---|
| 94 | 0.000 | 25.36% | 96 | 0.025 | 6.22% | 96 | 0.025 | 5.43% | 96 | 0.025 | 4.82% |
| 96 | 0.025 | 19.01% | 95 | 0.027 | 6.06% | 95 | 0.027 | 5.31% | 95 | 0.027 | 4.72% |
| 95 | 0.027 | 17.49% | 100 | 0.032 | 5.68% | 100 | 0.032 | 5.01% | 100 | 0.032 | 4.47% |
| 100 | 0.032 | 14.09% | 97 | 0.057 | 4.25% | 97 | 0.057 | 3.85% | 72 | 0.123 | 3.65% |
| 99 | 0.032 | 7.11% | 94 | 0.000 | 4.18% | 72 | 0.123 | 3.76% | 97 | 0.057 | 3.52% |
| 97 | 0.057 | 5.38% | 72 | 0.123 | 3.86% | 94 | 0.000 | 3.55% | 76 | 0.130 | 3.40% |
| 101 | 0.045 | 4.21% | 98 | 0.070 | 3.64% | 76 | 0.130 | 3.48% | 60 | 0.140 | 3.09% |
| 98 | 0.070 | 3.22% | 76 | 0.130 | 3.54% | 98 | 0.070 | 3.35% | 98 | 0.070 | 3.09% |
| 72 | 0.123 | 0.78% | 60 | 0.140 | 3.16% | 60 | 0.140 | 3.14% | 94 | 0.000 | 3.08% |
| 76 | 0.130 | 0.59% | 77 | 0.141 | 3.13% | 77 | 0.141 | 3.11% | 77 | 0.141 | 3.07% |

*Table S2: A list of the ten most probable bulk configurations of $Pt_2Pd_3$ predicted by SOD,101 inequivalent configurations at different temperatures listing the configuration numbers, relative electronic bulk energies and Boltzmann probabilities*

| Config. No. | 25 °C Relative Energy (kJ) | Probability (%) | Config. No. | 700 °C Relative Energy (kJ) | Probability (%) | Config. No. | 800 °C Relative Energy (kJ) | Probability (%) | Config. No. | 900 °C Relative Energy (kJ) | Probability (%) |
|---|---|---|---|---|---|---|---|---|---|---|---|
| 94 | 0.000 | 25.36% | 94 | 0.000 | 6.22% | 94 | 0.000 | 5.43% | 94 | 0.000 | 4.82% |
| 95 | 0.071 | 19.01% | 95 | 0.071 | 6.06% | 95 | 0.071 | 5.31% | 95 | 0.071 | 4.72% |
| 97 | 0.091 | 17.49% | 97 | 0.091 | 5.68% | 97 | 0.091 | 5.01% | 97 | 0.091 | 4.47% |
| 98 | 0.097 | 14.09% | 98 | 0.097 | 4.25% | 98 | 0.097 | 3.85% | 98 | 0.097 | 3.65% |
| 96 | 0.105 | 7.11% | 96 | 0.105 | 4.18% | 96 | 0.105 | 3.76% | 96 | 0.105 | 3.52% |
| 93 | 0.141 | 5.38% | 93 | 0.141 | 3.86% | 93 | 0.141 | 3.55% | 93 | 0.141 | 3.40% |
| 101 | 0.163 | 4.21% | 73 | 0.241 | 3.64% | 73 | 0.241 | 3.48% | 73 | 0.241 | 3.09% |
| 66 | 0.187 | 3.22% | 66 | 0.187 | 3.54% | 72 | 0.246 | 3.35% | 72 | 0.246 | 3.09% |
| 99 | 0.182 | 0.78% | 72 | 0.246 | 3.16% | 66 | 0.187 | 3.14% | 18 | 0.251 | 3.08% |
| 100 | 0.203 | 0.59% | 18 | 0.251 | 3.13% | 18 | 0.251 | 3.11% | 66 | 0.187 | 3.07% |

*Figure S1: Visualisation of (a) across and (b) onto views $Pt_3Pd_2$ configuration 3, including the (c) list of Cartesian coordinates of the 32 atom bulk*

a)

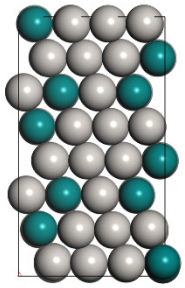

b)

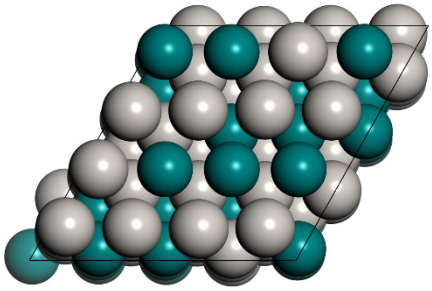

c)

| | x | y | z |
|---|---|---|---|
| Pd | 10.7295 | 9.4649 | 0.0000 |
| d | 5.3767 | 4.6678 | 0.0456 |
| Pd | 2.6202 | 4.6394 | 0.0468 |
| Pd | 13.4976 | 9.4406 | 0.1017 |
| Pt | 1.3160 | 2.2367 | 0.1242 |
| Pt | 9.4892 | 7.0486 | 0.1455 |
| Pd | 8.1057 | 4.5717 | 0.1500 |
| Pt | 14.8783 | 7.0736 | 0.1944 |
| Pt | 6.7919 | 7.0905 | 0.2022 |
| Pt | 8.0345 | 9.4438 | 0.2097 |
| Pt | 10.8101 | 4.6071 | 0.2139 |
| Pt | 12.2078 | 7.0777 | 0.2166 |
| Pt | 9.5434 | 2.3052 | 0.2433 |
| Pd | 16.2157 | 9.4463 | 0.2541 |
| Pt | 4.0862 | 2.3025 | 0.2889 |
| Pt | 6.7148 | 2.2360 | 0.3087 |
| Pt | 9.4732 | 8.6268 | 2.3421 |
| Pt | 12.1718 | 8.6192 | 2.3517 |
| Pt | 12.2300 | 3.8316 | 2.3592 |
| Pt | 13.5613 | 6.1753 | 2.3688 |
| Pt | 4.0164 | 3.8463 | 2.3922 |
| Pd | 5.3781 | 6.1974 | 2.3931 |
| Pt | 5.4097 | 1.3361 | 2.4048 |
| Pd | 10.8486 | 6.1869 | 2.4081 |
| Pd | 8.1207 | 6.1789 | 2.4084 |
| Pt | 6.7329 | 3.7567 | 2.4117 |
| Pd | 2.6918 | 1.3937 | 2.4186 |
| Pt | 14.8795 | 8.5470 | 2.4267 |
| Pt | 9.4653 | 3.7846 | 2.4291 |
| Pd | 8.1386 | 1.3728 | 2.4294 |
| Pd | 10.8759 | 1.4064 | 2.4561 |
| Pt | 6.7243 | 8.6045 | 2.4627 |

*Figure S2: Visualisation of (a) across and (b) onto views $Pt_2Pd_3$ configuration 17, including the (c) list of Cartesian coordinates of the 32 atom bulk*

a)

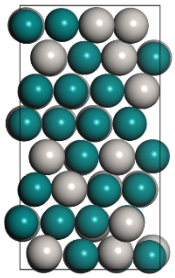

b)

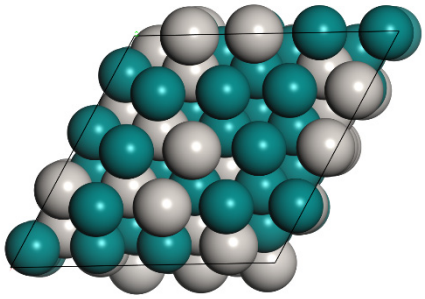

c)

| | x | y | z |
|---|---|---|---|
| Pd | 1.5116 | 0.7308 | 0.0000 |
| Pd | 4.2358 | 0.7551 | 0.0036 |
| Pd | 4.2235 | 5.4201 | 0.0069 |
| Pd | 8.1777 | 2.9808 | 0.0267 |
| Pd | 2.9623 | 7.9470 | 0.0417 |
| Pd | 1.5004 | 5.3084 | 0.0468 |
| Pd | 9.6632 | 0.7183 | 0.0672 |
| Pd | 6.9189 | 5.4958 | 0.0705 |
| Pd | 0.0797 | 7.9036 | 0.0765 |
| Pd | -1.2450 | 5.3516 | 0.1020 |
| Pt | 5.4899 | 3.1054 | 0.2292 |
| Pt | 5.7055 | 7.9080 | 0.2340 |
| Pt | 2.8604 | 3.1132 | 0.2472 |
| Pt | -2.7041 | 7.9122 | 0.2700 |
| Pt | 0.1133 | 3.0460 | 0.2766 |
| Pt | 6.8738 | 0.5356 | 0.3060 |
| Pt | 8.3232 | 4.5538 | 2.2149 |
| Pt | -1.2433 | 2.3034 | 2.2284 |
| Pt | -2.4529 | 9.3956 | 2.2506 |
| Pt | 2.9250 | 4.6352 | 2.2512 |
| Pt | 5.5592 | 4.6276 | 2.2566 |
| Pt | 0.1924 | 9.3822 | 2.2758 |
| Pd | 1.5265 | 7.0394 | 2.2968 |
| Pd | -5.1535 | 9.4400 | 2.3163 |
| Pd | 4.2829 | 6.9598 | 2.3175 |
| Pd | -1.2157 | 6.9830 | 2.3544 |
| Pd | 6.9402 | 2.2361 | 2.3628 |
| Pd | 4.2378 | 2.1814 | 2.3703 |
| Pd | 1.5126 | 2.2591 | 2.3838 |
| Pd | 2.9656 | 9.4879 | 2.4048 |
| Pd | 0.2042 | 4.6367 | 2.4087 |
| Pd | 6.9800 | 6.9128 | 2.4348 |

*Figure S3: Visualisation of (a) across and (b) onto views $Pt_2Pd_3$ configuration 81, including the (c) list of Cartesian coordinates of the 32 atom bulk*

a)

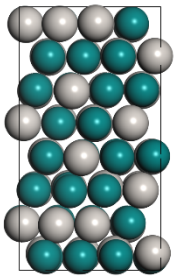

b)

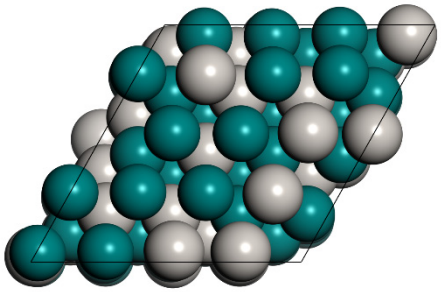

c)

| | x | y | z |
|---|---|---|---|
| Pd | 5.6760 | 6.5357 | 0.0000 |
| Pd | 9.7253 | 8.8229 | 0.0072 |
| Pd | 4.3828 | 4.0087 | 0.0126 |
| Pd | 9.7132 | 4.2000 | 0.0189 |
| Pd | 8.2728 | 1.8122 | 0.0291 |
| Pd | 12.4405 | 8.9387 | 0.0495 |
| Pd | 12.4970 | 4.1120 | 0.0522 |
| Pd | 6.9862 | 8.8923 | 0.0669 |
| Pd | 11.0780 | 1.6818 | 0.0735 |
| Pd | 13.7783 | 6.5308 | 0.1020 |
| Pt | 3.0519 | 1.6969 | 0.2037 |
| Pt | 7.0548 | 4.2859 | 0.2238 |
| Pt | 5.5193 | 1.6590 | 0.2616 |
| Pt | 8.3084 | 6.4752 | 0.2619 |
| Pt | 11.0794 | 6.4555 | 0.2640 |
| Pt | 15.0970 | 9.0050 | 0.3009 |
| Pt | 9.7335 | 2.4887 | 2.1930 |
| Pt | 11.1736 | 4.9229 | 2.2209 |
| Pt | 7.0080 | 7.3123 | 2.2257 |
| Pt | 5.7240 | 0.1750 | 2.2557 |
| Pt | 2.8344 | 4.9437 | 2.2566 |
| Pt | 8.4139 | 0.2359 | 2.2671 |
| Pd | 3.0115 | 0.1542 | 2.3151 |
| Pd | 5.6461 | 4.9722 | 2.3154 |
| Pd | 7.0131 | 2.5587 | 2.3277 |
| Pd | 1.5589 | 2.5626 | 2.3286 |
| Pd | 4.2980 | 7.3471 | 2.3514 |
| Pd | 12.4781 | 7.4012 | 2.3535 |
| Pd | 9.7363 | 7.3051 | 2.3793 |
| Pd | 0.2748 | 0.1330 | 2.4111 |
| Pd | 8.4854 | 4.9048 | 2.4120 |
| Pd | 4.2723 | 2.6237 | 2.4318 |

*Figure S4: Visualisation of (a) across and (b) onto views $Pt_2Pd_3$ configuration 8, including the (c) list of Cartesian coordinates of the 32 atom bulk*

a)

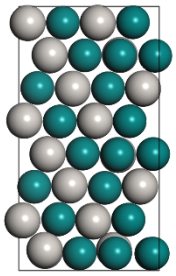

b)

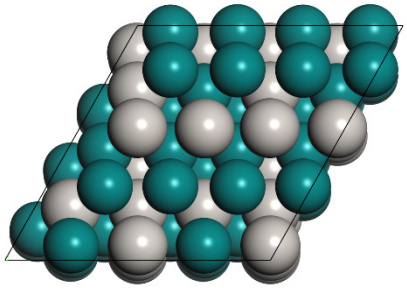

c)

| | x | y | z |
|---|---|---|---|
| Pd | 6.7343 | 9.0389 | 0.0000 |
| Pd | 12.1569 | 9.0389 | 0.0000 |
| Pd | 9.4904 | 4.1174 | 0.0075 |
| Pd | 4.0678 | 4.1174 | 0.0075 |
| Pd | 14.9055 | 9.1445 | 0.0123 |
| Pd | 9.4829 | 9.1445 | 0.0123 |
| Pd | 12.1821 | 4.1734 | 0.0252 |
| Pd | 6.7594 | 4.1734 | 0.0252 |
| Pd | 8.1529 | 6.5799 | 0.0339 |
| Pd | 13.5755 | 6.5799 | 0.0339 |
| Pt | 2.6093 | 1.7984 | 0.1878 |
| Pt | 8.0319 | 1.7984 | 0.1878 |
| Pt | 10.8265 | 6.4955 | 0.2502 |
| Pt | 5.4039 | 6.4955 | 0.2502 |
| Pt | 10.9160 | 1.7487 | 0.2511 |
| Pt | 5.4934 | 1.7487 | 0.2511 |
| Pt | 13.5887 | 5.0805 | 2.1852 |
| Pt | 8.1661 | 5.0805 | 2.1852 |
| Pt | 10.7999 | 5.0549 | 2.2410 |
| Pt | 5.3773 | 5.0549 | 2.2410 |
| Pt | 5.4183 | 0.2545 | 2.2563 |
| Pt | 10.8410 | 0.2545 | 2.2563 |
| Pd | 12.1891 | 7.4535 | 2.3121 |
| Pd | 6.7665 | 7.4535 | 2.3121 |
| Pd | 2.6811 | 0.2673 | 2.3142 |
| Pd | 8.1037 | 0.2673 | 2.3142 |
| Pd | 9.4925 | 7.4924 | 2.3211 |
| Pd | 14.9152 | 7.4924 | 2.3211 |
| Pd | 9.4934 | 2.6870 | 2.3235 |
| Pd | 4.0708 | 2.6870 | 2.3235 |
| Pd | 12.1810 | 2.7424 | 2.3697 |
| Pd | 6.7583 | 2.7424 | 2.3697 |